



# Fatigue life evaluation of welded joints in steel bridge considering residual stress



Chuang Cui<sup>a</sup>, Qinghua Zhang<sup>a,\*</sup>, Yi Bao<sup>b</sup>, Yizhi Bu<sup>a</sup>, Ying Luo<sup>a</sup>

<sup>a</sup> Department of Bridge Engineering, Southwest Jiaotong University, Chengdu, Sichuan 610031, China

<sup>b</sup> Department of Civil, Environmental and Ocean Engineering, Stevens Institute of Technology, 1 Castle Point Terrace, Hoboken, NJ 07030, USA

## ARTICLE INFO

### Article history:

Received 3 September 2018

Received in revised form 23 October 2018

Accepted 3 November 2018

Available online xxxx

### Keywords:

Fatigue crack propagation

Fatigue life

Fatigue tests

Steel truss

Welded joints

Weld residual stress

## ABSTRACT

Welded joints are widely used to connect structural components in steel truss bridges. Weld residual stresses (WRS) and weld residual stresses relaxation (WRSR) have notable influences on fatigue crack propagation in welded joints, and therefore affect the fatigue life of welded joints. Failing to properly consider the effect of WRS and WRSR in fatigue evaluation may lead to inaccurate results. This study presents a fatigue life prediction model based on the elastic fracture mechanics, with consideration of the WRS and WRSR. The solution for stress intensity factor caused by cyclic loading and WRS is derived. The WRS-induced stress intensity factor is calculated using a weight function technique. Fatigue tests of eight welded joint specimens are implemented, and the fatigue failure analysis of specimens is conducted. The proposed fatigue life prediction model is validated against fatigue test results of welded joints. By considering both WRS and WRSR, the model provides a prediction of fatigue life with a maximum error of 14%. Finally, the validated model is employed to investigate the fatigue life of a real bridge. The fatigue life is underestimated by 17% by considering WRS but not considering WRSR; the fatigue life is overestimated by 49% by neglecting WRS and WRSR.

© 2018 Elsevier Ltd. All rights reserved.

## 1. Introduction

Steel trusses are extensively used in highway and railway bridges. Fig. 1 shows the cross section of a typical steel truss girder [1–3]. Welded joints and high-strength bolts have been used to connect different bridge components, such as the top and bottom chords, verticals, diagonals, bracings, etc. In Fig. 1, an I-shape steel beam is welded on a gusset plate that connects the bottom chords, vertical and diagonals. It has been found that the fatigue resistance of welded joint, especially the connection of gusset and flange plates (named as T-shape welded joint), is susceptible to traffic loads, weld residual stresses (WRS), weld defects, and stress concentration, etc. [3–5]. However, methods for predicting the fatigue life of the welded joint with consideration of WRS and WRSR are still under development.

A lot of research efforts have been devoted to understanding the effect of WRS on fatigue failure. Sumi et al. [6] investigated the effect of WRS on fatigue life and failure paths through fatigue tests of butt welded plates. Galatolo and Lanciotti [7] reported that the WRS increased the growth rate of fatigue crack perpendicular to the weld line, reducing the fatigue life. Gerhard [8] established a formula to relate the WRS and crack growth threshold. Cui et al. [9] found that the WRS highly reduced the fatigue resistance of a steel bridge. Ultrasonic impact

treatment was used to increase the threshold of stress intensity factor and enhance the fatigue resistance [10,11]. In addition to the experimental studies, finite element analysis has been carried out to study the effect of WRS on the fatigue life of welded joints under cyclic loading [12]. Although the effect of WRS on the fatigue resistance of welded joints has been studied, there are limited studies on the relaxation of WRS, namely WRSR, which is a phenomenon that the WRS is partially released at the welded joints under cyclic loading [13–17]. WRSR is a complicated procedure governed by the interaction of the amplitude and range of stresses, loading scenario, loading cycles, material properties, etc. [14]. A reasonable estimation of WRSR is the prerequisite of predicting fatigue life of welded joints. Effective methods for analyzing the effect of WRSR on fatigue life of welded joints are yet to be developed.

This study aims to develop a fatigue life prediction model for estimating fatigue life of steel truss bridges with consideration of WRS and WRSR. The model is derived based on fracture mechanics for quantitative analysis of fatigue life, validated using test results from cruciform welded joint specimens, and finally used to evaluate the fatigue life of an in-service steel truss bridge.

## 2. Development of fatigue life model

To consider the effect of WRS and WRSR on fatigue life of welded joints of steel truss bridge, a fatigue life prediction model is developed

\* Corresponding author.

E-mail address: swjtuzqh@home.swjtu.edu.cn (Q. Zhang).

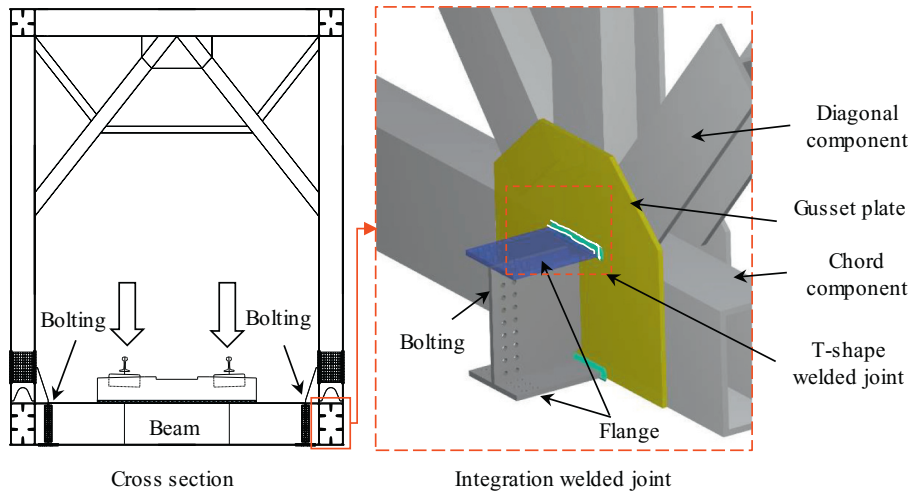


Fig. 1. Sketch of steel truss welded joint.

based on the linear elastic fracture mechanics. First, the effective stress intensity factor is determined considering the combined WRS and external loading. Then, crack propagation in welded joints is analyzed through linear elastic fracture mechanics. Finally, the fatigue life is predicted quantitatively.

2.1. Effective stress intensity factor

Considering the combined effect of the WRS and external loading, the effective stress intensity factor ( $K_{eff}$ ) is defined as [12]:

$$K_{eff} = K_s + K_r \tag{1}$$

where  $K_s$  and  $K_r$  are the stress intensity factors associated with the external cyclic loading and WRS, respectively.

According to BS7910:2005 [18],  $K_s$  is determined using Eq. (2):

$$K_s = M_K K_n \tag{2}$$

where  $K_n$  is the stress intensity factor in the same plate without any attachment, as shown in Fig. 2.  $M_K$  is a magnification factor [18] dependent on the type of the welded joint.

The stress intensity factor  $K_n$  in the plate without any attachment is determined using Eq. (3) according to [18]:

$$K_n = M_s(\lambda_1, \lambda_2, \lambda_3, \theta) \frac{\sigma_n \sqrt{\pi a}}{E_k} \quad (0 \leq a/c < 2, c/W < 0.5, 0 \leq \theta \leq \pi) \tag{3}$$

where  $\sigma_n$  is the nominal stress of welded joint under external mechanical loading;  $\lambda_1 = a/c$ ,  $\lambda_2 = a/t$ ,  $\lambda_3 = c/W$ ;  $a$  and  $c$  denote the crack width and half-length of crack, respectively;  $W$  is the half-width of cracked plate;  $\theta$  is weld angle;  $M_s$  is determined using Eq. (4):

$$M_s = [M_1 + M_2 \lambda_2^2 + M_3 \lambda_2^4] f_g f_\theta f_W \tag{4}$$

where the variables  $M_1$ ,  $M_2$ ,  $M_3$ ,  $f_g$ ,  $f_\theta$ , and  $E_k$  are determined by Eqs. (5) to (7):

When  $\lambda_1 \leq 1$ ,

$$\left. \begin{aligned} M_1 &= 1.13 - 0.09\lambda_1 \\ M_2 &= -0.54 + 0.89/(0.2 + \lambda_1) \\ M_3 &= 0.5 - 1/(0.65 + \lambda_1) + 14(1 - \lambda_1)^{24} \\ f_g &= 1 + (0.1 + 0.35\lambda_2^2)(1 - \sin\theta)^2 \\ f_\theta &= (\lambda_1 \cos\theta)^2 + \sin^2\theta \\ E_k &= (1 + 1.161\lambda_1^{1.65})^2 \end{aligned} \right\} \tag{5}$$

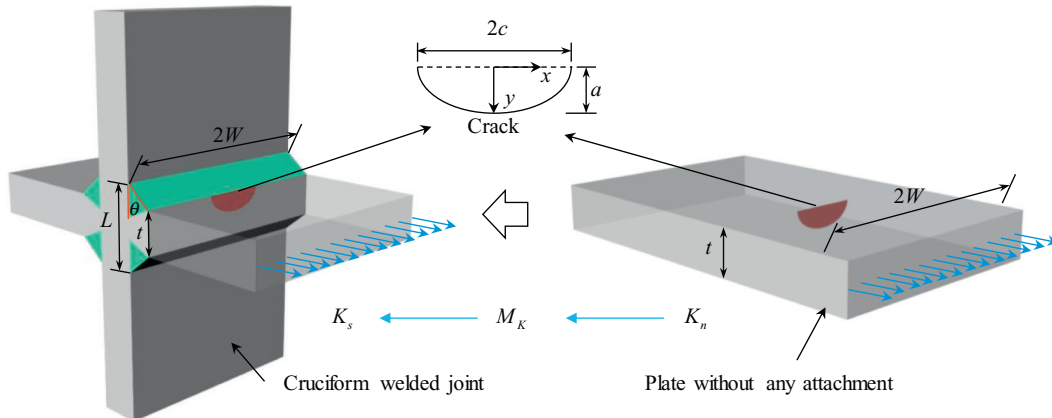


Fig. 2. The stress intensity factor of cruciform welded joints is determined using the stress intensity factor of the plate with any attachment.

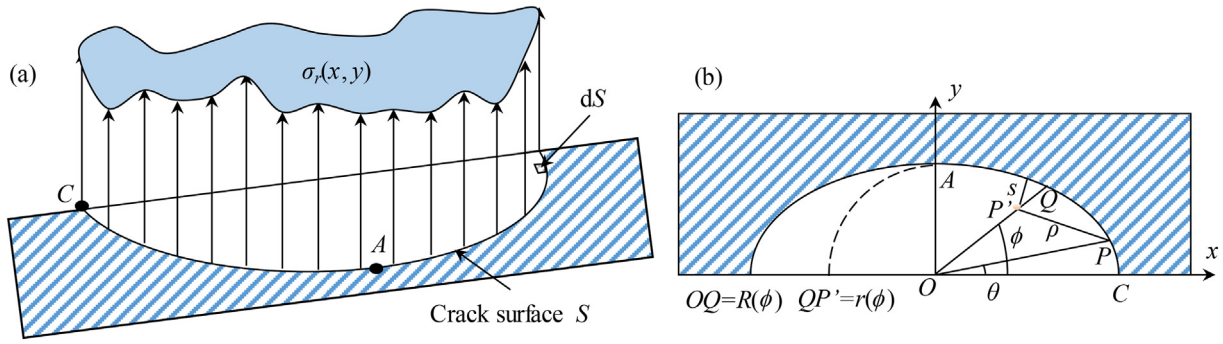


Fig. 3. Two-dimensional weight function for a semi-elliptical crack: (a) sketch of two-dimensional WRS distribution; (b) weight function notation.

When  $\lambda_1 > 1$ ,

$$\left. \begin{aligned} M_1 &= (1 + 0.04/\lambda_1)/\sqrt{\lambda_1} \\ M_2 &= 0.2\lambda_1^{-4} \\ M_3 &= -0.11\lambda_1^{-4} \\ f_g &= 1 + (0.1 + 0.35\lambda_2^2/\lambda_1)(1 - \sin\theta)^2 \\ f_\theta &= (\cos\theta/\lambda_1)^2 + \sin^2\theta \\ E_k &= (1 + 1.161\lambda_1^{-1.65})^2 \end{aligned} \right\} \quad (6)$$

$$f_W = \left[ \sec\left(\frac{\pi c}{2W}\right) \sqrt{\lambda_2} \right]^{\frac{1}{2}} \quad (7)$$

The simplified formula and intermediate parameters incorporating the different component geometries and loading conditions are investigated by Carpinteri et al. [19] and Lewandowski et al. [20]. The magnification factor  $M_K$  at weld toe or root is obtained through three-dimensional finite element analysis with consideration of weld geometry, loading condition and crack aspect ratio. In this study, the magnification factors of weld toe and weld root respectively proposed by Lie et al. [21] and Song et al. [22] are adopted:

$$M_K = f_s(\lambda_1, \lambda_2, \theta, \psi) \quad (8)$$

where  $f_s$  is the basic function [21,22];  $\psi$  is the ratio of the weld footprint width ( $L$ ), and thickness of plate ( $t$ ), as shown in Fig. 2.

To quantify the effect of WRS on the stress intensity factor, the weight function method is adopted to determine the WRS-induced stress intensity factor ( $K_r$ ) [23,24]:

$$K_r = \int \int \sigma_r(x, y) \cdot m(x, y; \phi) dS \quad (9)$$

where  $\sigma_r(x, y)$  is the WRS distribution across the crack surface in the unflawed body, as shown in Fig. 3(a);  $S$  is the crack surface;  $m(x, y; \phi)$  is a two-dimensional point-load weight function for any point along the crack front of a semi-elliptical surface crack. Wang and Glinka [25] formulated a general weight function for elliptical cracks in an infinite or semi-infinite body, and demonstrated the accuracy of the weight function for a wide range of crack types. Ghajar and Googarchin [24] derived the weight function for the semi-elliptical crack in the finite thickness plates:

$$m(x, y; P) = \frac{\sqrt{2s}}{\pi^{1.5}\rho^2} \left[ 1 + M(\lambda_1, \lambda_2, \phi) \left( 1 - \frac{r(\phi)}{R(\phi)} \right) \right] \quad (10)$$

where  $s$  is the shortest distance between the point load and the boundary of the crack front;  $\rho$  is the distance between load point  $P'$  and an arbitrary point  $P$  along the crack front.

The coefficient  $M(\lambda_1, \lambda_2, \phi)$  is a function of  $\lambda_1, \lambda_2$  and  $\phi$  [21,22];  $\phi$  is the angle between  $QP'$  and  $x$ -axis, as shown in Fig. 3(b);  $R(\phi)$  and  $r(\phi)$  are the distances of  $OQ$  and  $QP'$ , respectively, as shown in Fig. 3(b).

At an arbitrary point  $P$  along the crack front,  $K_r$  is determined using Eq. (11):

$$K_r(P) = \int \int \sigma_r(x, y) \frac{\sqrt{2s}}{\pi^{1.5}\rho^2} \left[ 1 + M(\lambda_1, \lambda_2, \phi) \left( 1 - \frac{r(\phi)}{R(\phi)} \right) \right] dS \quad (11)$$

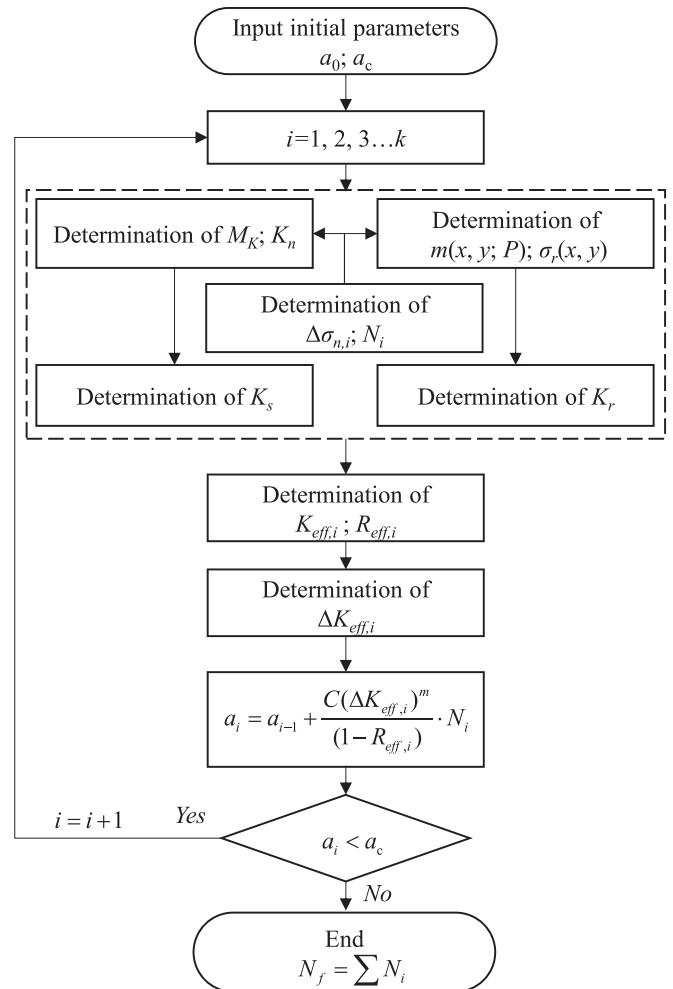


Fig. 4. Flow chart of fatigue life prognosis.

Table 1  
Parameters of the WRS relaxation model.

$\alpha_1$	$\alpha_2$	$\alpha_3$	$\alpha_4$
4.625	6.456	6.480	0.08789

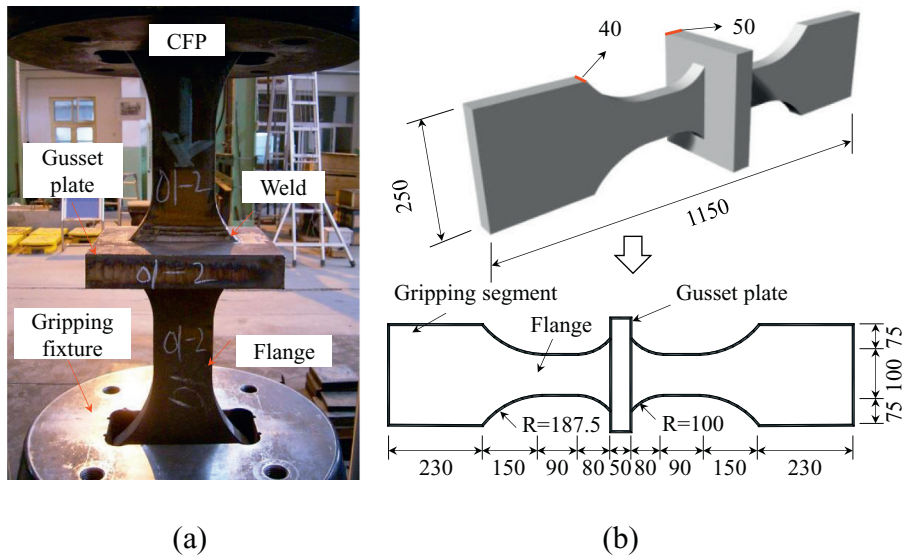


Fig. 5. Cruciform welded joint: (a) fatigue testing; (b) schematic illustration (unit: mm).

Under cyclic loading, WRS is partially released with increase of the loading cycle. The extent of relaxation is dependent on the stress ranges, number of loading cycles, loading scenario, and material properties [14]. Several models have been proposed to evaluate the degree of relaxation [15–17]. In this study, the WRSR model proposed by Xie et al. [16] is adopted. The WRS is represented by  $\sigma_r(x,y)$ , as expressed in Eq. (12):

$$\sigma_r(x,y) = \sigma_{r0}(x,y) - \sigma_{r0}(x,y) [\alpha_1 (\Delta\sigma_n/\sigma_s)^{\alpha_2} + \alpha_3] [\ln(N+1)]^{\alpha_4} \quad (12)$$

where  $\sigma_{r0}(x,y)$  is the initial WRS;  $\Delta\sigma_n$  is the nominal amplitude of the external cyclic stress;  $\sigma_s$  is the yielding stress;  $N$  is the number of loading cycles;  $\alpha_1$ ,  $\alpha_2$ ,  $\alpha_3$ , and  $\alpha_4$  are four material parameters that can be obtained by WRS measurement under mechanical cyclic loading. The parameters in Eq. (12) are determined based on a previous study [9], as listed in Table 1.

According to Eq. (12), the effect of WRSR can be considered in Eq. (11) to obtain WRS induced stress intensity factor  $K_r$  for any point  $P$  along the crack front.

## 2.2. Prediction of fatigue life

The effective intensity factor  $K_{eff}$  considering the combination of the cyclic loading and WRS can be expressed as Eq. (1). Hence, the range of effective intensity factor, denoted by  $\Delta K_{eff}$ , can be calculated as:

$$\Delta K_{eff} = K_{eff, \max} - K_{eff, \min} = (K_{s, \max} + K_r) - (K_{s, \min} + K_r) = \Delta K_s \quad (13)$$

where  $K_{eff, \max}$  and  $K_{eff, \min}$  respectively represent the maximum and minimum effective stress intensity factors;  $K_{s, \max}$  and  $K_{s, \min}$  are the maximum and minimum stress intensity factors associated with the external cyclic loading. When the calculated result of  $K_{eff, \min}$  is less than 0,  $K_{eff, \min}$  is taken as 0 to account for the effect of crack closure on crack

propagation [12]. Therefore, Eq. (13) can be rewritten as:

$$\Delta K_{eff} = \begin{cases} \Delta K_s & \text{for } K_{eff, \min} \geq 0 \\ K_{eff, \max} & \text{for } K_{eff, \min} < 0 \end{cases} \quad (14)$$

A crack propagation model that considers both the effective intensity factor range and the effective stress ratio [12] is adopted:

$$\frac{da}{dN} = \frac{C(\Delta K_{eff})^m}{(1-R_{eff})} \quad (15)$$

where  $C$  and  $m$  are the material constant;  $N$  is the number of cycles;  $R_{eff}$  which is the effective stress ratio with combination of WRS denotes as:

$$R_{eff} = \frac{K_{s, \min} + K_r}{K_{s, \max} + K_r} \quad (16)$$

It is noted that  $\Delta K_{eff}$  and  $R_{eff}$  vary with the external loading, WRS and crack length. An arbitrary cyclic loading history is addressed using a rainflow method [4] to obtain the sequences of the nominal stress range  $\Delta\sigma_n$  and the corresponding number of loading cycle  $N$ . Assuming that the  $i$ th nominal stress range and loading cycle are respectively  $\Delta\sigma_{n, i}$  and  $N_i$ , the  $i$ th effective stress intensity factor range  $\Delta K_{eff, i}$  and the  $i$ th effective stress ratio  $R_{eff, i}$  can be obtained by Eqs. (1) to (15). Then, the crack length  $a_i$  can be determined by the numerical integration of

Table 3  
Fatigue loading protocol and testing results.

Specimen ID	Nominal stress ranges (MPa)	Frequency (Hz)	Failure cycle	Location of crack initiation
1	140	4.5	78,400	Weld toe
2	130	3.5	950,400	Weld root
3	220	2.0	94,000	Weld toe
4	170	2.8	562,300	Weld root
5	120	3.5	2,000,000+	–
6	200	2.5	72,600	Weld toe
7	180	2.6	140,800	Weld root
8	150	3.2	474,200	Weld toe

Table 2  
Mechanical properties of Q370QD steel.

Thickness (mm)	Yield stress (MPa)	Ultimate tensile stress (MPa)	Elongation (%)
50	385	535	30
40	395	645	26

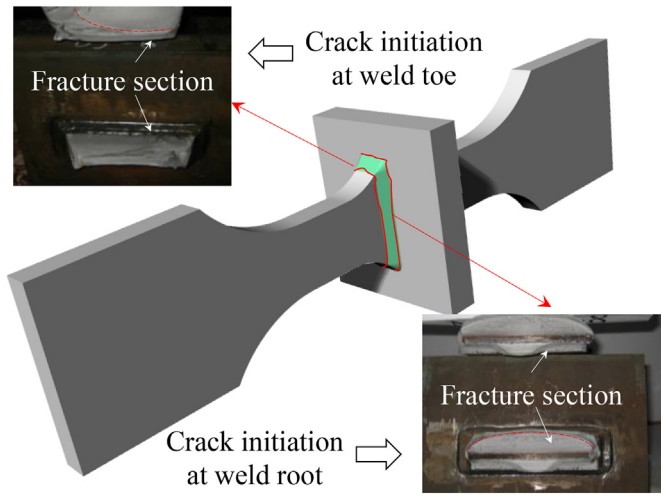


Fig. 6. Morphology of the fatigue fracture surface of the cruciform welded joints.

Eq. (16) as follows:

$$a_i = a_{i-1} + \frac{C(\Delta K_{eff,i})^m}{(1-R_{eff,i})} \cdot N_i \quad (17)$$

It is assumed that the given initial and critical crack length are respectively  $a_0$  and  $a_c$ . If  $a_i$  is greater than  $a_c$  after the  $k$ th numerical integration of Eq. (17), the structure is regarded as failure. Finally, the fatigue life  $N_f$  can be predicted by Eq. (18) and the following flow chart in Fig. 4.

$$N_f = \sum_{i=1}^k N_i \quad (18)$$

### 3. Validation of fatigue life prediction model

#### 3.1. Fatigue tests

Fatigue tests of welded joints were conducted to validate the fatigue life prediction model. Fig. 5 shows the cruciform joints that were tested to simulate the T-shape welded joint shown in Fig. 1 [11]. The test specimens were made of hot-rolled low alloy steel Q370qD [3], which is a structural steel for bridges. Table 2 shows the manufacturer specified mechanical properties of the steel plates with different thicknesses. The information for cyclic loading and fatigue testing results are listed in Table 3. The fifth specimen did not fail after it experienced more than 2 million loading cycles. It is noted that the constant amplitudes

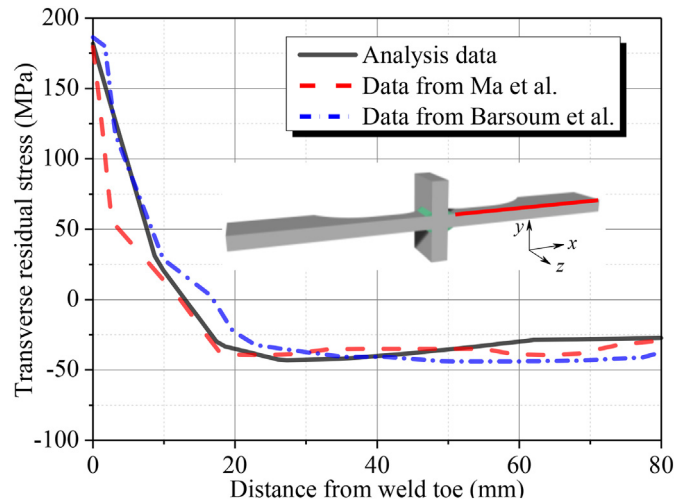


Fig. 8. Transverse residual stress distribution at the flange surface.

of nominal stress were used in the fatigue tests, and the minimum value of cyclic stresses was set as 2 MPa consistently.

The finite element analysis shows that the stress concentration is more severe at the weld toe than that at the weld root for cruciform welded joints [26]. Table 2 shows that the failure cycle of the specimens whose crack initiation location is at the weld toe is dramatically less than the specimens whose crack initiation location is at the weld root. This is likely due to the initial defects and a higher stress concentration at the weld toe.

The typical failure modes are shown in Fig. 6. The failure surface is a quarter or half ellipse. The weld defects and stress concentration are the predominant causes of crack initiation, but the crack growth rate that determines the fatigue life depends on the external cyclic loading and WRSR because of the welding heterogeneity [14].

#### 3.2. Model validation

##### 3.2.1. Weld residual stress

A thermo-mechanical analysis is conducted to analyze the WRS using finite element codes in ANSYS. First, heat transfer analysis is performed to determine the temperature distribution in the welded joints. Second, mechanical analysis is conducted to determine the stress distributions in the welded joints, based on the temperature distributions determined through the heat transfer analysis. Temperature-dependent thermal and mechanical material properties [4] of the steel are adopted. Mesh size convergence study was performed, and a global mesh size of 4 mm was adopted. Gradually-varied, the meshing size of 2 mm at the weld is refined to ensure the computational accuracy, as shown in Fig. 7. The three translational degrees of freedom at the nodes ( $x = 0$  mm and  $x = 1150$  mm) of gripping segment zone were constrained.

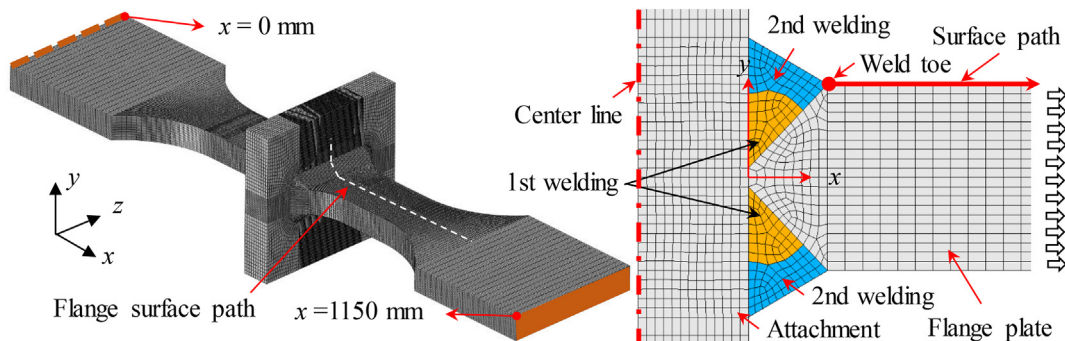


Fig. 7. Finite element model of cruciform welded joint for WRS analysis.

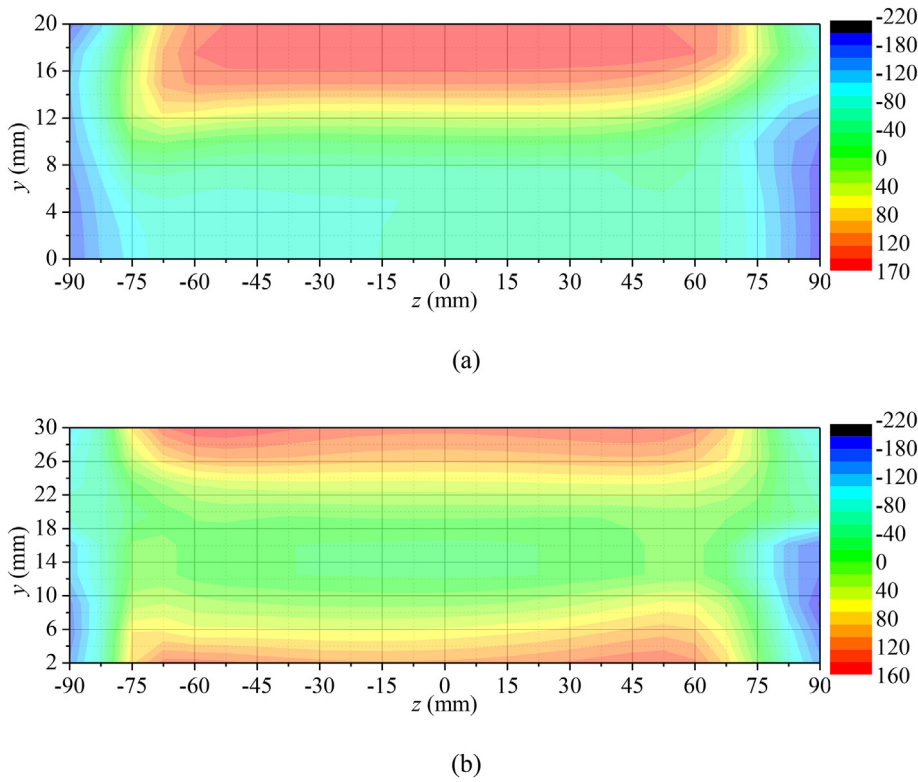


Fig. 9. Contours of WRS (unit: MPa) in Specimen 2 at the cross sections of: (a) weld toe; (b) weld root.

A volumetric heat source with a double ellipsoidal distribution was used [4]. The front and rear heat sources are respectively described using Eqs. (19) and (20).

$$q(x, y, z, t) = \frac{6\sqrt{3}f_f Q}{a_1 b c \pi \sqrt{\pi}} e^{-3(z-vt-z_0)^2/a_1^2} e^{-3x^2/b^2} e^{-3y^2/c^2} \quad (19)$$

$$q(x, y, z, t) = \frac{6\sqrt{3}f_r Q}{a_2 b c \pi \sqrt{\pi}} e^{-3(z-vt-z_0)^2/a_2^2} e^{-3x^2/b^2} e^{-3y^2/c^2} \quad (20)$$

where  $f_f$  and  $f_r$  are constants which give the fractions of the heat deposited in the front and rear of the weld bead, respectively;  $Q$  is the magnitude of the heat input per unit time, and it could be calculated according to the arc voltage, arc current and arc efficiency;  $v$  is the welding

speed;  $t$  is the welding time;  $z_0$  is the position of the heat source along the  $z$ -direction at  $t = 0$ ;  $a_1$ ,  $a_2$ ,  $b$ , and  $c$  are parameters dependent on the welding arc ( $a_1 = 2.0$  mm,  $a_2 = 4.0$  mm,  $b = 1.2$  mm, and  $c = 1.0$ ) [4].

Fig. 8 shows the WRS represented by the maximum principle stress along the  $x$ -axis (Fig. 7). Due to lack of the direct measurement data of WRS, the numerical simulation results of WRS in [12,27] are used to validate the numerical simulations in this study, because of their consistent welding procedure parameters and boundary conditions. The WRS analysis data is consistent with the data from Ma et al. [27] and Barsoum et al. [12], validating the finite element model for quantification of the WRS.

Figs. 9(a) and 9(b) respectively show the WRS at the crack sections of the weld toe and weld root in the Specimen 2. The WRS varies from

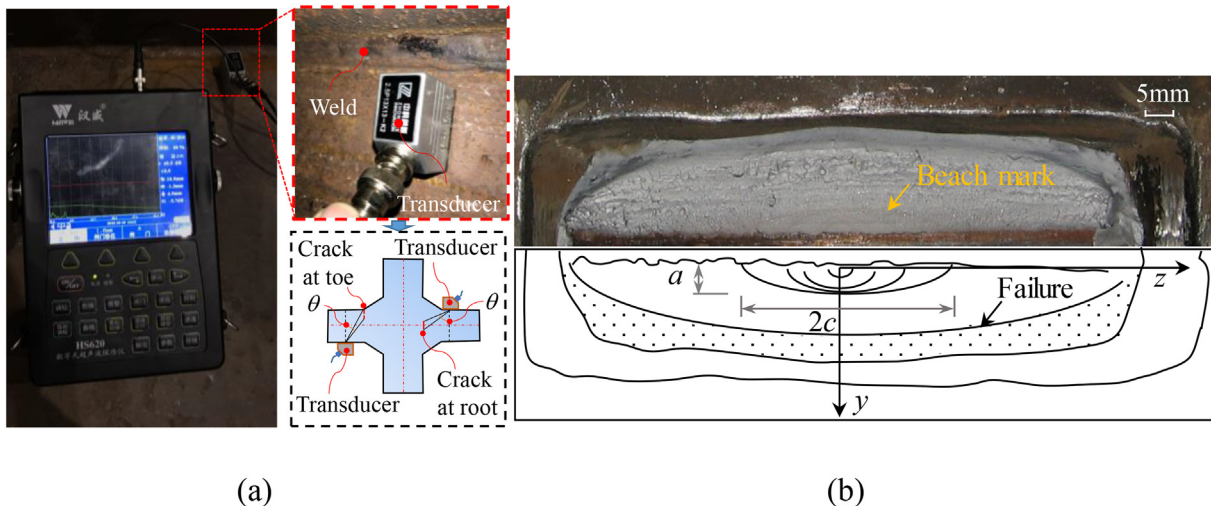


Fig. 10. Fatigue crack propagation monitoring: (a) crack length measurement; (b) fracture surface of specimen 2.

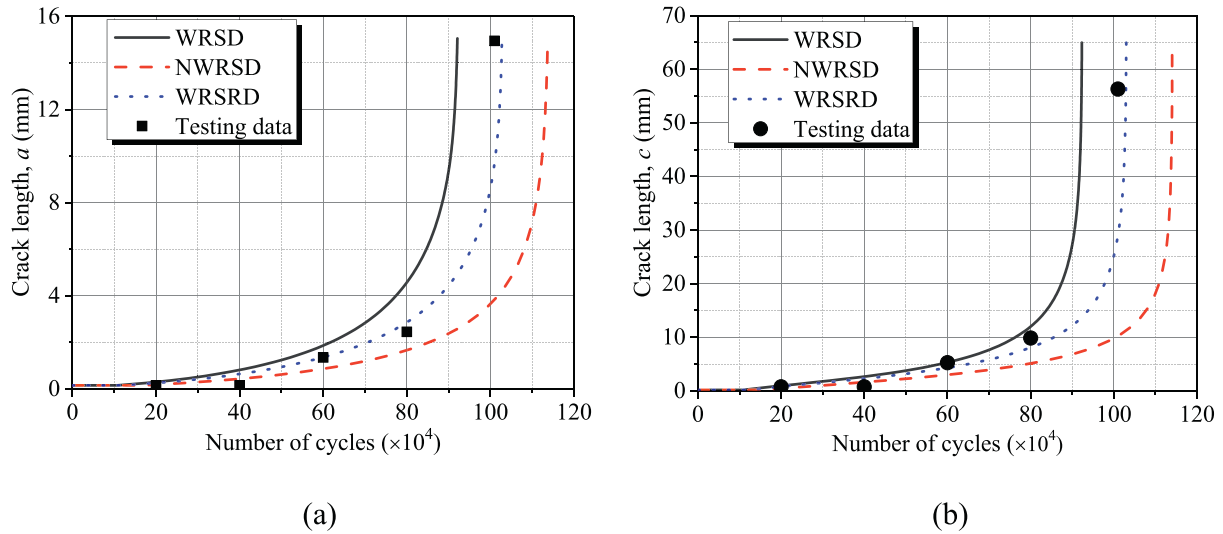


Fig. 11. Comparison of tested and predicted lifetimes: (a)  $a$ - $N$ ; (b)  $c$ - $N$ .

–200 MPa (in compression) to 170 MPa (in tension) in the same cross section. The maximum tensile WRS occurs at the weld toe and root, which are also subjected to stress concentration and initial welding defects. The combined effects facilitate initiation of fatigue crack.

3.2.2. Validation of fatigue life prediction

The Specimen 2 is analyzed to expound the crack propagation process under external cyclic stress considering the WRS and WRSR. The ultrasonic detection method [28] was used to measure the fatigue crack with the increase of cycles, as shown in Fig. 10(a). And the measurement method introduced in [28] was adopted in this study. The fracture surface of Specimen 2 and semi-elliptical fatigue cracks were examined along the weld root line, as shown in Fig. 10(b).

The specimen failed as the normal section of weld root plane reached the limit of the bearing capacity with the growth of crack. The crack length and crack width are critical values at final failure of specimens. It is assumed that the initial crack length and crack width are 0.15 mm [29]. The material constants  $C$  and  $m$  of Q370qD for crack propagation are  $4.41 \times 10^{-12}$  and 2.98 [30], respectively. The magnification factor  $M_K$  in Eq. (3) is recommended in [21,22]. The weight function  $m(x, y; P)$  for welded joints is given in [23,24]. The simulation of crack propagation is conducted by using the validated fatigue life prediction model. Figs. 11(a) and 11(b) show the analysis results and test data of crack length of specimen 2 with the increase of number of cycles.

In Fig. 11, “WRS” is the analysis result that considers the WRS and does not consider the WRSR; “WRSR” is the analysis result that considers both WRS and WRSR; “NWRSD” is the analysis result that does not consider the WRS nor WRSR. Besides, those analysis results are obtained by the same fatigue life prediction model with or without consideration of WRS in Eq. (1). The prediction results considering WRS and WRSR show better agreement with the test data. Not considering WRS

and WRSR overestimates the fatigue life; only considering WRS but not considering WRSR underestimates the fatigue life.

The predicted results are listed in Table 4. The result of the Specimen 5 is not included, because the specimen did not fail. For the analysis results that considers both the WRS and WRSR, the maximum relative error is 14%, while the maximum relative error is up to 210% as the WRS and WRSR are not considered.

4. Case study

To exemplify the use of the proposed fatigue life prediction model, an in-service truss bridge with a simple span of 100 m is analyzed using in-situ monitoring data. The width and thickness of the flange plate are 480 mm and 40 mm, respectively. The weld type and process of the welded joints are same as that in the fatigue tests to ensure the consistency of initial WRS. Five fatigue details at the joints WJ-1 to WJ-5 are analyzed, as shown in the three-dimensional finite element model in Fig. 12(a). The model has 530 nodes and 486 beam elements. The model is established for the influence line analysis of the welded joints. The influence line of the stress perpendicular to the weld line ( $x$ -axis) at each of the five joints is shown in Fig. 12(b).

The shapes of different influence lines are similar except for the peak stress. The nominal stress ranges of different welded joints are close. A qualitative identification of trains was implemented to obtain the database of traffic volumes provided from the railway administration. The standard components of traffic mixes are shown in Fig. 13, and the unit ‘t’ stands for ton. The fatigue load spectrum is determined by the database of traffic volumes, as listed in Table 5.

The stochastic traffic loads were generated by Monte-Carlo method based on the statistical traffic volumes in Table 4. The nominal stress histories at the welded joints under the stochastic traffic loads can be

Table 4 Comparison of the predicted results and test data.

Cycles and error	Specimen ID							
	1	2	3	4	6	7	8	
Prediction (WRSRD)	69,450	890,000	100,530	592,320	81,360	152,000	539,000	
Relative error (%)	11	6	7	5	12	8	14	
Prediction (WRS)	53,660	703,000	50,500	436,259	45,990	100,760	416,000	
Relative error (%)	32	26	46	22	37	28	12	
Prediction (NWRSD)	201,320	980,000	205,400	783,200	101,680	436,400	568,320	
Relative error (%)	157	3	119	39	40	210	20	

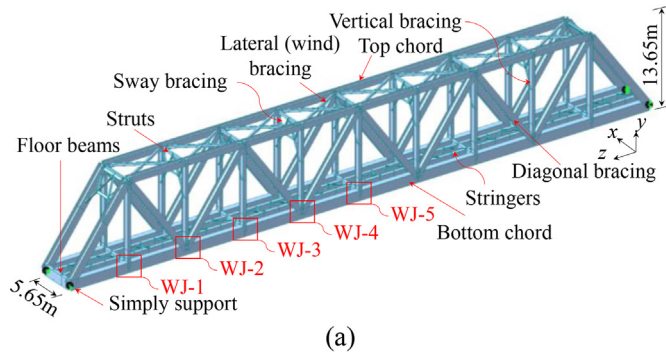


**Table 5**  
Fatigue load spectrum obtained by the monitoring data.

Types of trains	ID	Standard traffic mixes	Mass of trains (ton)	Number of trains per year	Traffic volume (million ton/year)
Freight trains	TF1	L1 + 9A + 2B + 17C + 9D + 2E	3253	2356	7.66
	TF2	L2 + 13A + 2B + 22C + 12D + 3E	4312	1576	6.80
	TF3	L1 + 34C + 19D	3468	1039	3.60
	TF4	L2 + 28C + 14D	4341	696	3.02
	TF5	L1 + 48E	3070	566	1.74
	TF6	L2 + 40E	3671	371	1.36
Passenger trains	TP1	L1 + 19F	972	1604	1.56
	TP2	L2 + 15F	1210	1076	1.30

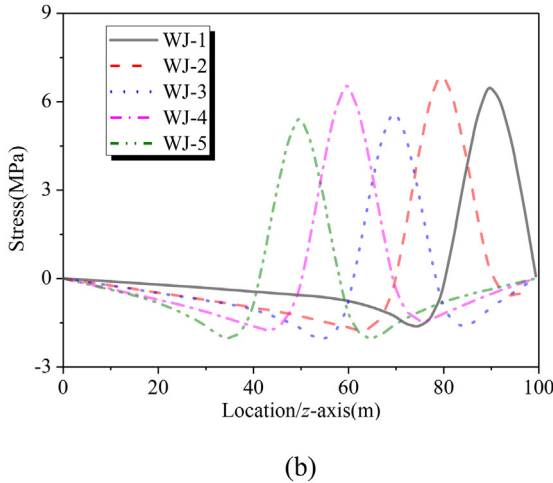


**Fig. 12.** Finite element analysis: (a) finite element model; (b) influence lines of the stress perpendicular to the weld line at WJ-1 to WJ-5.

obtained by influence lines and stochastic traffic loads. The nominal stress history of welded joint WJ-1 is shown in Fig. 14.

Based on the fatigue life prediction model, the crack propagation process of welded joints can be predicted by the fracture mechanics. The crack growth of the welded joint WJ-1 is illustrated as an example in Fig. 15. The fatigue failure is defined as the appearance of penetrated crack along the thickness of flange plate ( $a_c = 20$  mm) in this case study. Fig. 15 reveals that the fatigue life is overestimated by not considering the WRS, and underestimated by considering WRS but not WRSR.

The fatigue life of the welded joints (WJ-1 to WJ-5) is predicted, as depicted in Fig. 16. The predicted fatigue life with WRS varies from 95 years to 105 years under stochastic traffic loads, while fatigue life without consideration of WRS ranges from 163 years to 206 years. The

prediction life with WRSR is from 111 years to 131 years. Compared to the average fatigue life with WRSR (122 years), the average fatigue life with WRS (101 years) is underestimated by 17%, while the average fatigue life without WRS (182 years) is overrated by 49%.

It is worth noting that the fatigue evaluation of the bridge is a complicated problem and needs more research efforts. The case study of the steel truss bridge aims to exemplify the use of the proposed fatigue life evaluation method and manifest the effect of WRS and WRSR on the fatigue life of the bridge. Further research is needed to establish a holistic understanding and assess the fatigue life of the bridge.

**5. Conclusions**

A fatigue life prediction model with consideration of both WRS and WRSR based on elastic fracture mechanics is proposed to evaluate the fatigue life of welded joints. The proposed method is validated through fatigue tests and exemplified through a case study of a steel truss bridge. The main conclusions are summarized as follows:

- (1) The fatigue life prediction model based on the elastic fracture mechanics is developed to evaluate the fatigue life of welded joints considering effect of WRS and WRSR. The fatigue tests of cruciform welded joints are carried out to validate the accuracy of fatigue life prediction model. The growth of crack width and crack length with consideration of WRS and WRSR are in good agreement with the testing data. In addition, the predicted fatigue life is in line with the failure cycles with a 14% of maximum relative error, demonstrating the applicability and accuracy of the fatigue life prediction model.
- (2) A case study of steel truss bridge exemplifies the proposed fatigue life evaluation method and manifests the effect of WRS and WRSR on the fatigue life of the bridge. Fatigue life is

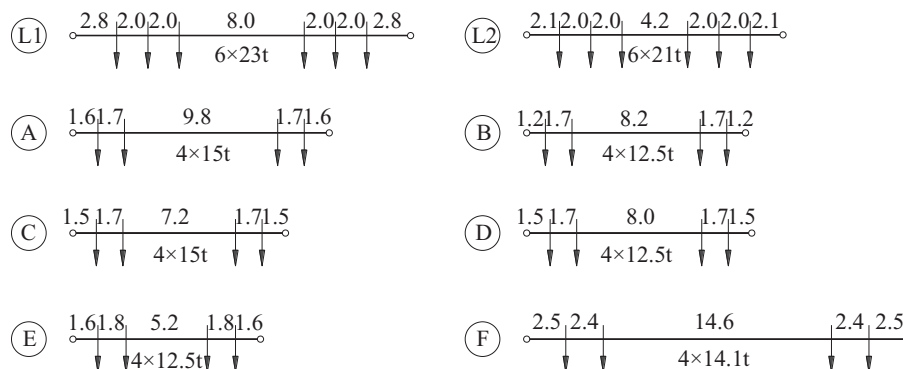


**Fig. 13.** Types of standard components of traffic mixes (unit: m).

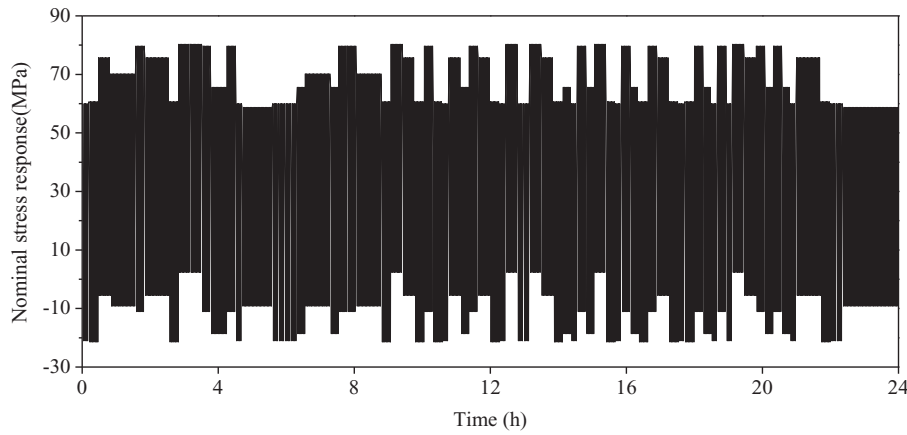


Fig. 14. Nominal stress history of welded joint (WJ-1).

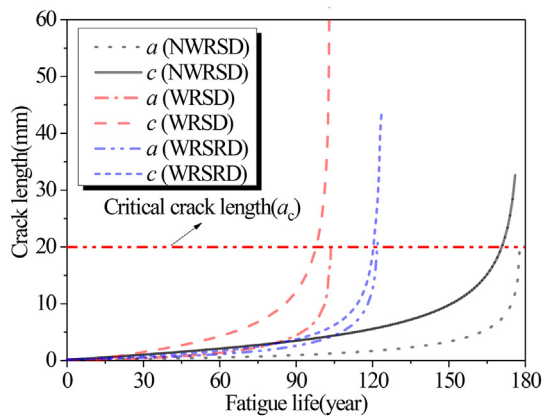


Fig. 15. Crack propagation of welded joint (WJ-1).

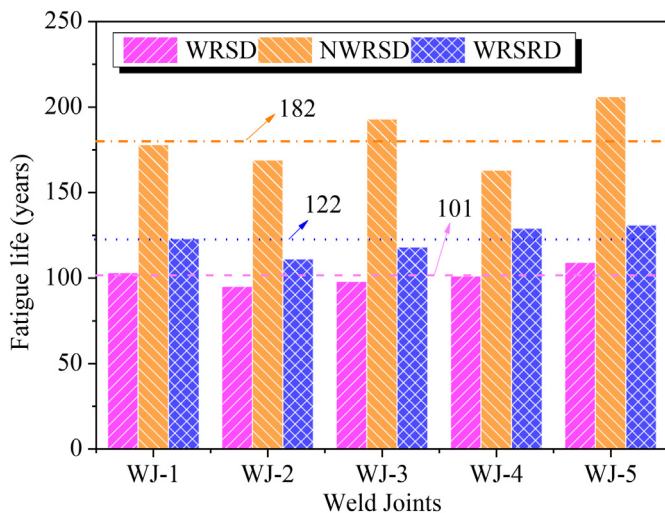


Fig. 16. Prediction of fatigue life based on the traffic loads.

overestimated without considering WRS and WRSR. The comparison of results shows that there is a 17% reduction in fatigue life considering WRS without WRSR, and a 49% increase in fatigue life neglecting WRS and WRSR, compared with the fatigue life with WRS and WRSR.

### Acknowledgments

This research was funded by the National Natural Science Foundation of China [grant numbers 51778533, 51878561, 51578455, 50908192, and 51178394], Fundamental Research Funds for the Central Universities [grant number 2682014CX078], Science and Technology Program of Hubei Transportation Department [grant number 2017-538-2-4] and National Science and Technology Support Program of China [grant number 2011BAG07B03].

### References

- [1] B. Cheng, Q. Qian, H.T. Sun, Steel truss bridges with welded box-section members and bowknot integral joints, part II: minimum weight optimization, *J. Constr. Steel Res.* 80 (2013) 475–482.
- [2] Q. Pu, H. Wang, H. Gou, Y. Bao, M. Yan, Fatigue behavior of prestressed concrete beam for straddle-type monorail tracks, *Appl. Sci.* 8 (7) (2018) 1136.
- [3] X. Wei, L. Xiao, S. Pei, Fatigue assessment and stress analysis of cope-hole details in welded joints of steel truss bridge, *Int. J. Fatigue* 100 (2017) 136–147.
- [4] Cui, C., Bu, Y., Bao, Y., Zhang, Q., Ye, Z. Strain energy-based fatigue life evaluation of deck-to-rib welded joints in OSD considering combined effects of stochastic traffic load and welded residual stress, *J. Bridg. Eng.*, 2018, 23(2): 04017127–1–15.
- [5] C. Cui, Q. Zhang, Y. Luo, H. Hao, J. Li, Fatigue reliability evaluation of deck-to-rib welded joints in OSD considering stochastic traffic load and welding residual stress, *Int. J. Fatigue* 111 (2018) 151–160.
- [6] Y. Sumi, C. Yang, Z.N. Wang, Morphological aspects of fatigue crack propagation Part II - effects of stress biaxiality and welding residual stress, *Int. J. Fract.* 82 (3) (1996) 221–235.
- [7] R. Galatolo, A. Lanciotti, Fatigue crack propagation in residual stress fields of welded plates, *Int. J. Fatigue* 19 (1) (1997) 43–49.
- [8] G. Biallas, Effect of welding residual stresses on fatigue crack growth thresholds, *Int. J. Fatigue* 50 (6) (2013) 10–17.
- [9] C. Cui, Q. Zhang, Y. Bao, Y.Z. Bu, Z.T. Ye, Fatigue damage evaluation of orthotropic steel deck considering weld residual stress relaxation based on continuum damage mechanics, *J. Bridg. Eng.* 23 (10) (2018), 04018073.
- [10] X. Cheng, J.W. Fisher, H.J. Prask, T. Gnäupel-Herold, B.T. Yen, S. Roy, Residual stress modification by post-weld treatment and its beneficial effect on fatigue strength of welded structures, *Int. J. Fatigue* 25 (9–11) (2003) 1259–1269.
- [11] C. Cui, Q. Zhang, Y. Bao, J. Kang, Y. Bu, Fatigue performance and evaluation of welded joints in steel truss bridges, *J. Constr. Steel Res.* 148 (2018) 450–456.
- [12] Z. Barsoum, I. Barsoum, Residual stress effects on fatigue life of welded structures using LEFM, *Eng. Fail. Anal.* 16 (1) (2009) 449–467.
- [13] W.Z. Zhuang, G.R. Halford, Investigation of residual stress relaxation under cyclic load, *Int. J. Fatigue* 23 (1) (2001) 31–37.
- [14] C.H. Lee, K.H. Chang, V.N.V. Do, Finite element modeling of residual stress relaxation in steel butt welds under cyclic loading, *Eng. Struct.* 103 (2015) 63–71.
- [15] J.C. Kim, S.K. Cheong, H. Noguchi, Residual stress relaxation and low- and high-cycle fatigue behavior of shot-peened medium-carbon steel, *Int. J. Fatigue* 56 (11) (2013) 114–122.
- [16] X.F. Xie, W. Jiang, Y. Luo, S. Xu, J.M. Gong, S.T. Tu, A model to predict the relaxation of weld residual stress by cyclic load: experimental and finite element modeling, *Int. J. Fatigue* 95 (2017) 293–301.
- [17] H.J. Yi, Y.J. Lee, Numerical analysis of welding residual stress relaxation in high-strength multilayer weldment under fatigue loads, *Metall. Mater. Trans. B Process Metall. Mater. Process. Sci.* 48 (4) (2017) 2167–2175.

- [18] B.S.I.B.S. 7910, Guide to Methods for Assessing the Acceptability of Flaws in Metallic Structures, British Standards Institution, 2005.
- [19] A. Carpinteri, R. Brighenti, H.J. Huth, S. Vantadori, Fatigue growth of a surface crack in a welded T-joint, *Int. J. Fatigue* 27 (1) (2005) 59–69.
- [20] J. Lewandowski, D. Rozumek, Numerical analysis of stress intensity factor in specimens with different fillet geometry subjected to bending, *Acta Mech. Autom.* 12 (1) (2018) 38–43.
- [21] S.T. Lie, S.P. Vipin, T. Li, New weld toe magnification factors for semi-elliptical cracks in double-sided T-butt joints and cruciform X-joints, *Int. J. Fatigue* 80 (2015) 178–191.
- [22] Z. Song, Y. Xiong, J. Xie, J.T. Xing, Weld root magnification factors for semi-elliptical cracks in T-butt joints, *Acta Mech. Solida Sin.* 26 (3) (2013) 317–330.
- [23] T. Fett, D. Munz, Stress Intensity Factors and Weight Functions, Computational Mechanics Publications, Southampton, 1997.
- [24] R. Ghajar, H.S. Googarchin, General point load weight function for semi-elliptical crack in finite thickness plates, *Eng. Fract. Mech.* 109 (2013) 33–44.
- [25] X. Wang, G. Glinka, Determination of approximate point load weight functions for embedded elliptical cracks, *Int. J. Fatigue* 31 (11–12) (2009) 1816–1827.
- [26] G. Meneghetti, P. Lazzarin, The peak stress method for fatigue strength assessment of welded joints with weld toe or weld root failures, *Weld. World* 55 (7–8) (2011) 22–29.
- [27] N.X. Ma, Y. Ueda, H. Murakawa, H. Maeda, FEM analysis of 3-D welding residual stresses and angular distortion in T-type fillet welds, *Trans. JWRI* 24 (2) (1995) 115–122.
- [28] S.C. Her, S.T. Lin, Non-destructive evaluation of depth of surface cracks using ultrasonic frequency analysis, *Sensors* 14 (9) (2014) 17146–17158.
- [29] A.F. Hobbacher, The new IIW recommendations for fatigue assessment of welded joints and components—a comprehensive code recently updated, *Int. J. Fatigue* 31 (1) (2009) 50–58.
- [30] Y.P. Liu, C.Y. Chen, G.Q. Li, Fatigue crack growth and control of 14MnNbq welding plates used for bridges, *J. Eng. Mech.* 138 (1) (2011) 30–35.